POLITECNICO DI TORINO
Repository ISTITUZIONALE

Data fusion in structural health monitoring: Integrating computer vision and strain gauges for enhanced inspection

(Article begins on next page)

26 November 2024

Data fusion in structural health monitoring: Integrating computer vision and strain gauges for enhanced inspection

K. Aminfar, M. Ghyabi, Y. Shen & D. Lattanzi
George Mason University, USA

G. Ciaramella, M. Gherlone & C. Surace
Politecnico di Torino, Italy

ABSTRACT: In the evolving field of Structural Health Monitoring (SHM), the integration of diverse sensing techniques is pivotal for comprehensive structural analysis. This study introduces a novel data fusion methodology that synergizes the precision of strain gauges with the broad coverage of computer vision techniques. Aimed at advancing SHM practices, our approach facilitates a detailed understanding of structural behavior by concurrently analyzing strain fields and displacement signals captured through video streams. We employ Physics Informed Neural Networks (PINNs) to refine measurements and ensure physical plausibility in our data interpretation. Our methodology's effectiveness is validated through laboratory experiments on a simplified structural model, demonstrating enhanced accuracy and reliability in SHM. This paper highlights the potential of integrating traditional and contemporary sensing techniques in infrastructure monitoring, setting a new benchmark in the field.

1 INTRODUCTION

Structural Health Monitoring (SHM) is vital for ensuring the integrity and safety of key infrastructures. Conventionally, SHM has heavily relied on direct sensor installations like strain gauges (Mousa et al., 2021). These sensors are indispensable as they not only detect, localize, and quantify unusual structural behaviors but also project current and future structural predictions (Glisic, 2022). Nevertheless, their deployment poses logistical challenges and often require multiple sensors for single-point displacement estimation (Ma et al., 2023), prompting the need for alternative methods.

Shifting focus, non-contact methods like utilizing video streams offer a valuable alternative. These methods capture displacement fields, reflecting the overall stiffness of structures and providing an accurate assessment of structural conditions (Feng & Feng, 2018). Despite their precision, vision-based techniques are not without drawbacks, including high computational demands and sensitivity to lighting conditions (Ma et al., 2023). Alone, these methods may fall short of the accuracy and consistency achieved through sensor-based approaches.

To address these challenges, our study proposes a multi-modal sensor fusion strategy. Traditional fusions generally combine accelerometers with either strain sensors or vision cameras (Ma et al., 2023). Our approach goes further, merging strain gauge data with computer vision outputs. This fusion integrates the precision of strain measurements with the extensive spatial analysis offered by video-based techniques. The aim is to develop a robust analytical framework that correlates strain and visual data, thus enriching SHM with a more comprehensive understanding of structural behavior.

Further advancing our methodology, we introduce Physics-Informed Neural Networks (PINNs) (Raissi et al., 2019) into our vision-based SHM framework. PINNs represent

a significant evolution from traditional machine learning models, as they offer enhanced interpretability and conform more closely to physical principles (Faroughi et al., 2023). By incorporating physical laws into the neural network architecture, PINNs ensure that the model's predictions are not only accurate but also physically plausible. Their application in SHM is multifaceted: for instance, they have been effectively utilized in modeling stress and displacement under varying conditions, an aspect central to understanding structural behaviors (Henkes et al., 2022). Furthermore, PINNs show promise in accurately simulating the behavior of materials under different strain rates and temperatures, a factor crucial for assessing the long-term durability and resilience of infrastructure (Arora et al., 2022). Importantly, PINNs have the capability to refine wave velocity estimations from displacement data, enhancing the precision of structural imaging and enabling the early detection of potential structural failures (Rathod & Ramuhalli, 2022). Additionally, their adeptness in solving complex differential equations relevant to structural dynamics positions them as an invaluable tool in SHM, particularly for analyzing intricate structural responses under varied load conditions (Kollmannsberger et al., 2021).

Overall, this study presents a novel approach in SHM by leveraging the combined strengths of both strain gauges and computer vision, further augmented by the analytical prowess of PINNs. This unique combination not only promises to bolster the accuracy and reliability of structural assessments but also signifies a substantial advancement in the application of machine learning within the domain of infrastructure monitoring.

2 METHODOLOGY

2.1 *Theoretical foundation*

In SHM, leveraging the strengths of different sensors is key to achieving comprehensive monitoring. Strain sensors offer high-precision local measurements, crucial for detecting minute changes in structural integrity. In contrast, vision-based methods provide extensive spatial coverage, enabling the capture of broader deformation patterns. This fusion approach is vital for a holistic understanding of structural condition.

A core aspect of our methodology involves shape sensing, which reconstructs a structure's displacement field using discrete surface strain measurements (Gherlone et al., 2018). According to the Bernoulli-Euler theory of pure bending, there is a direct correlation between axial strain and the curvature of the beam (Ko et al., 2007). This relationship is mathematically expressed as $\kappa = d^2w/dx^2$, where κ represents the curvature, and $w(x)$ denotes the beam's deflection along its longitudinal axis. The axial strain (ϵ) at any point is linked to curvature by $\epsilon = -y\kappa$, with 'y' being the distance from the neutral axis.

Using this principle, curvature is deduced from localized strain measurements. Subsequent numerical integration allows us to calculate the beam's slope (dw/dx) and overall deflection ($w(x)$). The precision of these estimations hinges on the density of strain data points, the accuracy of the numerical integration method, well-defined boundary conditions, and an exact characterization of the beam's properties and loading.

Utilizing the strain data recorded by our sensors, we augment our analysis by contrasting these sensor-derived displacement values at specific sensory points against the displacement data acquired through vision-based displacement measurement techniques.

2.2 *Image based displacement measurement*

To facilitate vision-based displacement measurement, the Demons algorithm is employed. The Thirion's image matching algorithm (Thirion, 1998), known as the Demons algorithm, is a linear complexity technique for nonrigid image registration, crucial in applications requiring intense value preservation. The proposed algorithm consists of estimation of the demon forces for every demon (more precisely, the result of the application of a force during one iteration step, that is a deformation field), and update of the transformation based on the calculated forces (Sotiras et al., 2013).

The core of the Demons algorithm lies in its optical flow component, which calculates pixel displacements by comparing sequential images. This comparison relies on the assumption of constant brightness over time, enabling accurate estimation of pixel movement between images. Essentially, the algorithm computes the displacement needed at each pixel (treated as a "demon") to align the moving image with the reference image. This calculation involves analyzing intensity gradients and differences between pixels.

In implementing this method, our study involved converting each frame into grayscale to standardize intensity values, followed by applying normalization techniques to ensure uniformity across images, countering variations in illumination. This preprocessing set the stage for the effective application of the Demons algorithm.

For enhanced efficiency and accuracy, a pyramidal approach is employed. This involves performing multiple iterations at progressively coarser image resolutions, starting with a low-resolution overview and gradually refining the displacement field at finer scales. This multi-scale approach balances computational efficiency with detailed displacement estimation (Zitová & Flusser, 2003).

2.3   Physics informed neural network

Physics-Informed Neural Networks (PINNs) (Raissi et al., 2019) operate by incorporating physical laws into the neural network architecture and its loss function, and aim to approximate solutions that closely match both the training data and the underlying physical equations. Here, the SciANN (Haghighat & Juanes, 2021), a Keras/TensorFlow wrapper is employed to create the PINN model.

2.3.1 Network architecture and data fitting
The architecture of the PINN is based on a standard feed-forward neural network (Kollmannsberger et al., 2021). The network is designed to predict displacement and strain as a function of the position along the beam, taking into account the beam's length (L), applied load (P), and material properties such as the modulus of elasticity (E) and moment of inertia (I).

To train the network, a synthesized dataset is created using analytical solutions for displacement and strain under various loading conditions. The data is further augmented by adding Gaussian noise, to mimic the real scenario. The data-fitting loss, L_{data}, is formulated as the mean squared error between the network's predictions and the actual values from the dataset. It is expressed as:

$$L_{data} = \left(\frac{1}{N}\right) \sum_1^N \left(\hat{d}_{(x_i)} - d_{data(x_i)}\right)^2 + \left(\hat{\varepsilon}_{(x_i)} - \varepsilon_{data(x_i)}\right)^2$$

where N is the number of data points, $\hat{d}$ and $\hat{\varepsilon}$ are the network's predictions for displacement and strain, respectively, and subscript *data* refers to the corresponding true values.

2.3.2 Incorporation of physical laws
The distinct feature of a PINN is its ability to integrate physical laws into the learning process. This is achieved by adding terms to the loss function that represent the governing equations of the system being modeled.

For a cantilever beam under a point load P, the Euler-Bernoulli beam theory provides the necessary physical laws. The physics-based loss for deflection, $L_{deflection}$, ensures the network's compliance with the deflection equation of the beam. It is given by:

$$L_{deflection} = \left(\frac{1}{M}\right) \sum_1^M \left(\hat{d}_{(x_i)} - \frac{Px_i^2}{6EI}(3L - x_i)\right)^2$$

Strain in a beam is directly related to its curvature, and the curvature at any point along the beam is mathematically represented by the second derivative of displacement with respect to

the position. Similarly, the physics-based loss for strain, L_{strain}, enforces the correct strain profile as per the beam theory. It is calculated as:

$$L_{strain} = \left(\frac{1}{M}\right) \sum_1^M \left(\hat{\varepsilon}_{(x_i)} - \frac{d^2\hat{d}}{dx^2}(x_i)\right)^2$$

where the term corresponding to the second derivative of the predicted displacement, indicates the curvature of the beam.

2.3.3 Total loss function and training

The overall loss function, L, for the PINN is a weighted sum of the data-fitting loss and the physics-based losses. It is defined as:

$$L_{total} = \alpha L_{data} + \beta L_{deflection} + \gamma L_{strain}$$

Here, α, β, and γ are coefficients that balance the importance of fitting the data and adhering to the physical laws.

2.4 Data fusion

The process begins with the calculation of the beam displacement field from the image sequence, designated as $v(z)$. This computation is conducted first through conventional image pre-processing, encompassing image cropping, selection of the Region of Interest, black weight artifact removal, and illumination correction. Following these initial steps, the punctual displacements are determined using the Demon algorithm, as previously stated. Then, the longitudinal strain field, termed $\varepsilon(z)$, is derived directly from the previously calculated displacement field, $v(z)$.

The refinement process involves enhancing the strain field, now referred to as $\varepsilon_{fix}(z)$, utilizing data from strain gauges. The displacement field, denoted as $v_{fix}(z)$, is then fine-tuned by numerically integrating this enhanced strain field, $\varepsilon_{fix}(z)$. An important assumption is the consideration of zero displacements at the beam ends. The interpolation of the displacement field employs smoothing splines. This stage is followed by a re-interpolation process, wherein an adjusted smoothing parameter is utilized to give precedence to data smoothness.

The computation of $\varepsilon(z)$ involves transforming the displacement data into strain data, guided by the principles of Hooke's and Navier's laws. The strain field, $\varepsilon_{fix}(z)$, is then calculated using a smoothing spline interpolation function. This function is designed to fit the data accurately and detect changes in slope, ensuring adherence to these changes. The computation of the refined displacement field is achieved through the double integration of linear functions. This process necessitates the imposition of boundary and continuity conditions.

2.5 Experimental setup and testing procedure

Our experimental investigation was conducted on a 6063 Aluminum beam, with dimensions of 50.80 mm width, 18.50 mm height, 1.60 mm thickness, and 2414.6 mm length. The beam was instrumented with six Type I strain gauges, arranged in a half-bridge configuration at intervals of L/4, L/2, and 3L/4 along the beam (Figure 1). This configuration, known for its high sensitivity and ability to compensate for temperature variations, ensured accurate strain measurement. Data from the strain gauges were captured using an NI cDAQ-9188 system, complemented by an optoNCDT 1420 laser sensor and an industrial-grade Ueye camera for deflection and motion tracking. To enhance image processing, the beam was marked with a colored speckle pattern, facilitating optical flow computations, and was positioned against a whiteboard for optimal contrast (Figure 2). The laser sensor acted as ground truth data for the investigations.

The experimental procedure involved a series of controlled static load tests with pinned ends to simulate hinge connections. The objective was to examine the beam's structural response to different load intensities, focusing on consistency and repeatability. Each test was conducted thrice to ensure the reliability of the data. The testing scenarios included 0.05, 0.2 and 0.5 kg load the beam's midpoint.
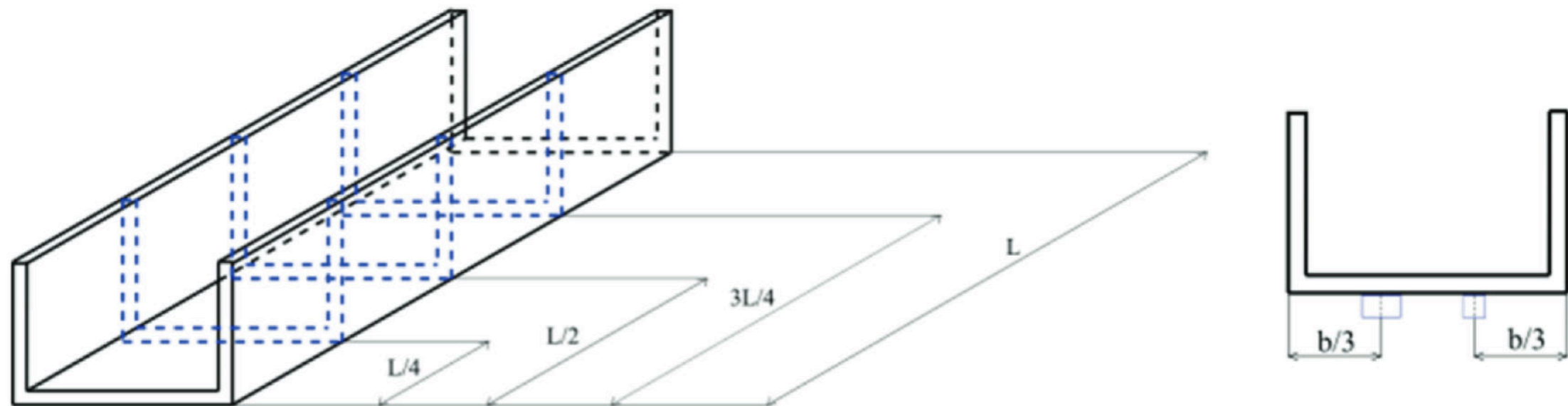

Figure 1.   Beam section and strain gauge locations.

Figure 2.   Experimental setup.

3   RESULTS AND DISCUSSION

This section presents the findings from our experimental tests, focusing on displacement and strain measurements under a 0.2 kg load at the centerline of the beam (Case 2), as these were typical for all conducted experienced. The results are illustrated in Figures 3 to 6.

Figure 3 displays the displacement curve obtained using the Image-based Measurement (IIm) method for Case 2. This graph results from iterative interpolation using smoothing splines, with the exclusion of residuals exceeding a set tolerance. The graph features an error measure focusing on data point fitting to the spline, along with a roughness measure:

$$p \sum_i w_i (y_i - s(z_i))^2 + (1 - p) \int \lambda \left(\frac{d^2 s}{dz^2} \right)^2 dz$$

Figure 4 illustrates the strain curve derived from both strain gauge readings and the analytical approach for Case 2. The stress-displacement relationship is characterized as

$$\frac{d^2 v(z)}{dz^2} = -\frac{\varepsilon(z)}{Y}$$

713

by assuming zero second derivatives at the beam's extremes. This accounts for the beam's properties as slender, elastic, and isotropic, with shear effects neglected.

The results of the corrected strain field, integrating strain gauge measurements, are presented in Figure 5. The process involves iterative and weighted interpolation with smoothing splines, exclusion of data points that degrade the distribution, and enforcement of interpolation at strain gauge measurements. Correction is applied based on the boundary condition of zero strain at the clamp section.

The comparison of the neural network's performance with and without the inclusion of the physics-based loss function is depicted in Figure 6. It is evident that the incorporation of the physics-based loss function enhances the model's generalizability and alignment with the physical phenomena for both strain and deflection.
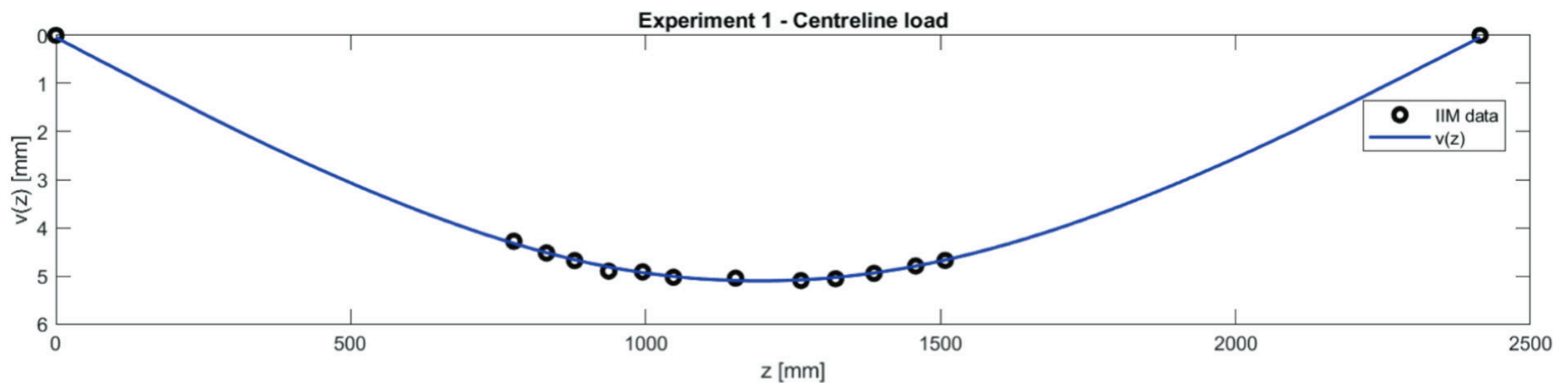

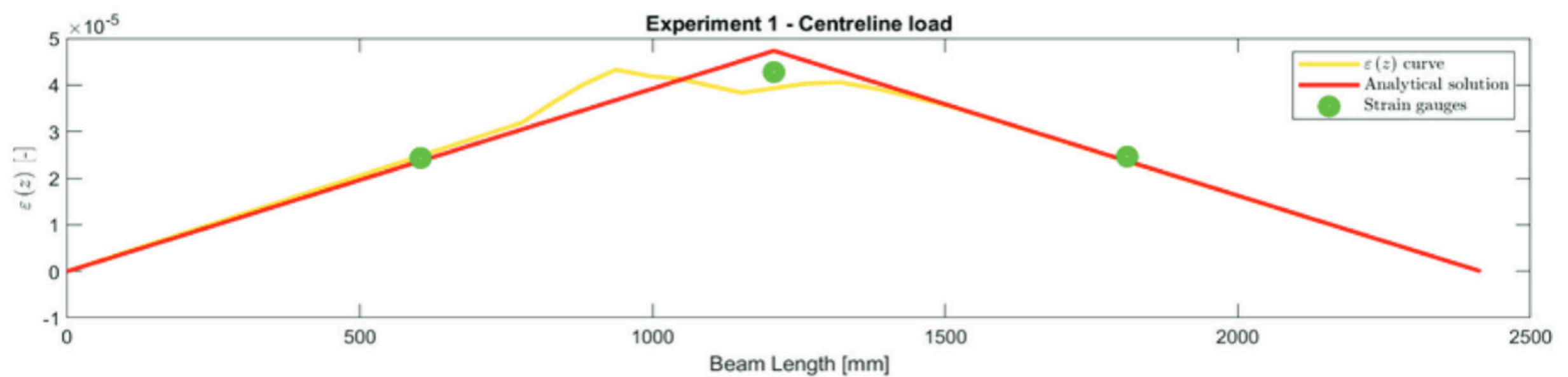Figure 3.   Image-based displacement measurement.

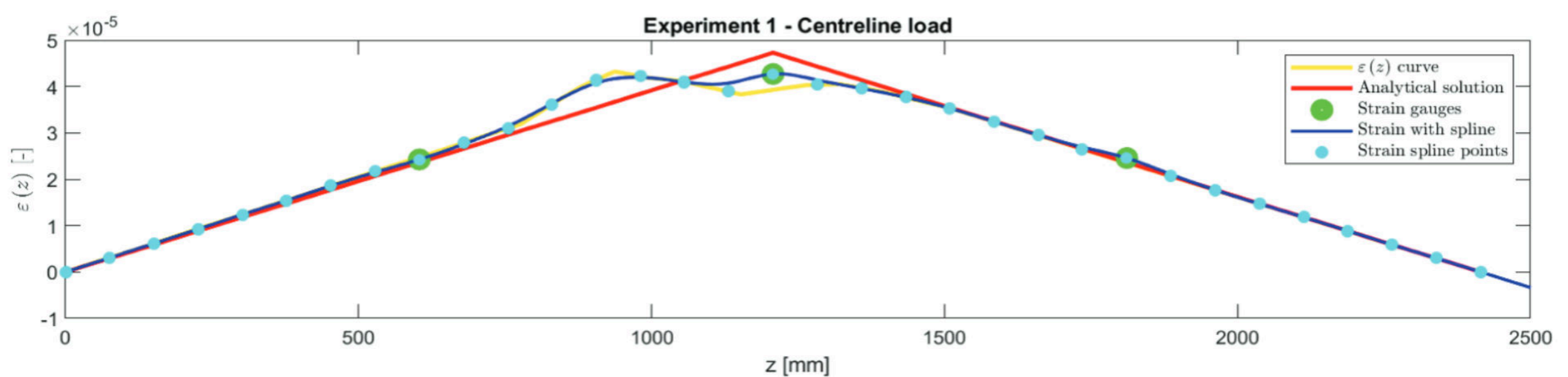Figure 4.   Strain analysis with strain gauges and analytical method.

Figure 5.   Corrected strain field with strain gauge measurements.

4   CONCLUSION

This study introduces an innovative approach that effectively combines strain gauge data and computer vision with an underlying physical formulation. Our method represents a significant advancement over traditional SHM techniques, particularly in its ability to accurately assess
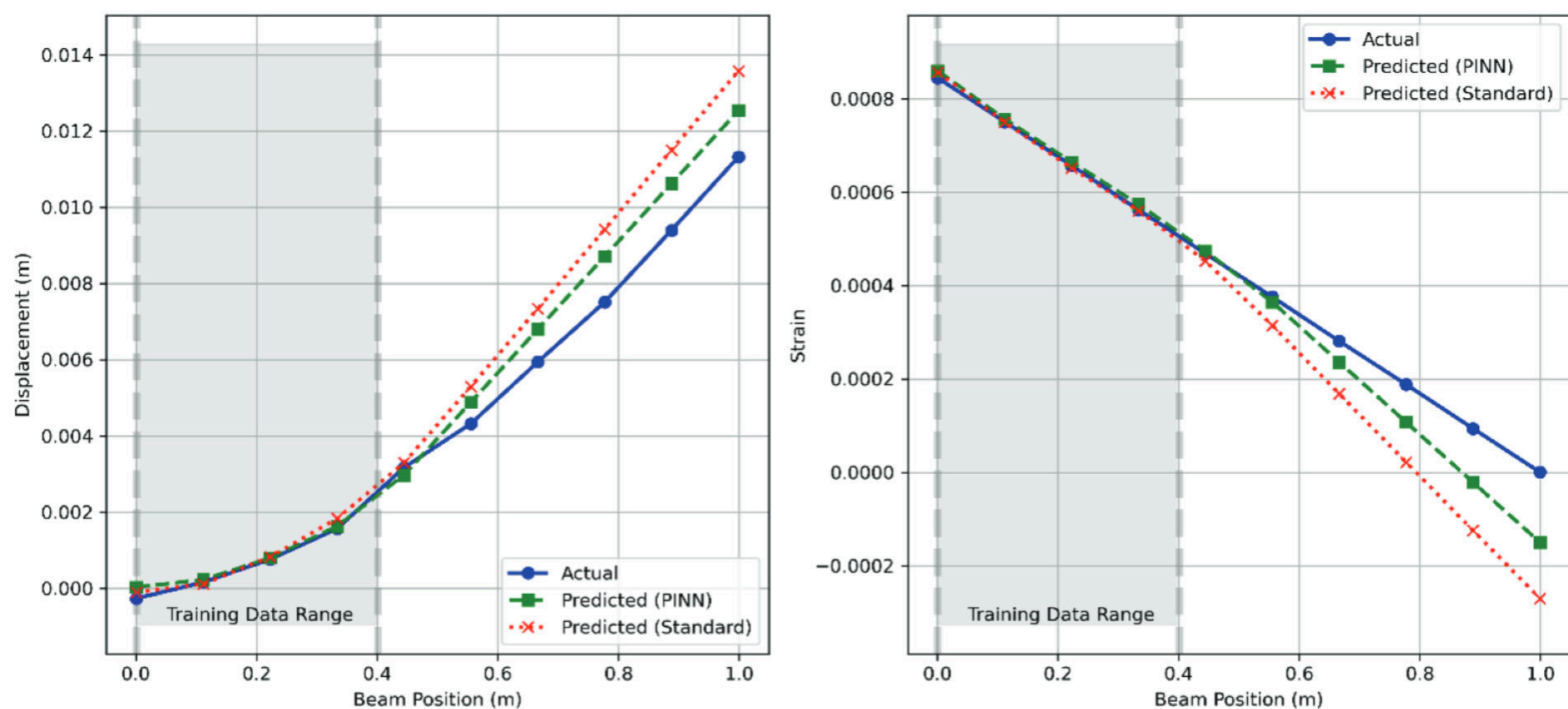
Figure 6.   Neural network performance with and without physics-based loss function.

structural integrity. This is achieved by correlating displacement and strain data through corrected measurements. The incorporation of Physics-Informed Neural Networks (PINNs) substantially enhances the accuracy and physical plausibility of the predictions, ensuring close alignment with actual structural responses under various load conditions. While our approach is effective in standard configurations, future work could aim to further enhance and integrate the model's accuracy in more complex structural scenarios, particularly through the application of PINNs. Such advancements promise to broaden the applicability of this innovative approach in the field of SHM.

REFERENCES

Arora, R., Kakkar, P., Dey, B., & Chakraborty, A. (2022). *Physics-informed neural networks for modeling rate- and temperature-dependent plasticity* (arXiv:2201.08363). arXiv. https://doi.org/10.48550/arXiv.2201.08363

Faroughi, S. A., Pawar, N., Fernandes, C., Raissi, M., Das, S., Kalantari, N. K., & Mahjour, S. K. (2023). *Physics-Guided, Physics-Informed, and Physics-Encoded Neural Networks in Scientific Computing* (arXiv:2211.07377). arXiv. http://arxiv.org/abs/2211.07377

Feng, D., & Feng, M. Q. (2018). Computer vision for SHM of civil infrastructure: From dynamic response measurement to damage detection – A review. *Engineering Structures*, *156*, 105–117. https://doi.org/10.1016/j.engstruct.2017.11.018

Gherlone, M., Cerracchio, P., & Mattone, M. (2018). Shape sensing methods: Review and experimental comparison on a wing-shaped plate. *Progress in Aerospace Sciences*, *99*, 14–26. https://doi.org/10.1016/j.paerosci.2018.04.001

Glisic, B. (2022). Concise Historic Overview of Strain Sensors Used in the Monitoring of Civil Structures: The First One Hundred Years. *Sensors*, *22*(6), Article 6. https://doi.org/10.3390/s22062397

Haghighat, E., & Juanes, R. (2021). SciANN: A Keras/Tensorflow wrapper for scientific computations and physics-informed deep learning using artificial neural networks. *Computer Methods in Applied Mechanics and Engineering*, *373*, 113552. https://doi.org/10.1016/j.cma.2020.113552

Henkes, A., Wessels, H., & Mahnken, R. (2022). Physics informed neural networks for continuum micromechanics. *Computer Methods in Applied Mechanics and Engineering*, *393*, 114790. https://doi.org/10.1016/j.cma.2022.114790

Ko, W. L., Richards, W. L., & Tran, V. T. (2007). *Displacement Theories for In-Flight Deformed Shape Predictions of Aerospace Structures*.

Kollmannsberger, S., D'Angella, D., Jokeit, M., & Herrmann, L. (2021). Physics-Informed Neural Networks. In S. Kollmannsberger, D. D'Angella, M. Jokeit, & L. Herrmann (Eds.), *Deep Learning in Computational Mechanics: An Introductory Course* (pp. 55–84). Springer International Publishing. https://doi.org/10.1007/978-3-030-76587-3_5

Ma, Z., Choi, J., & Sohn, H. (2023). Structural displacement sensing techniques for civil infrastructure: A review. *Journal of Infrastructure Intelligence and Resilience*, *2*(3), 100041. https://doi.org/10.1016/j.iintel.2023.100041

Mousa, M. A., Yussof, M. M., Udi, U. J., Nazri, F. M., Kamarudin, M. K., Parke, G. A. R., Assi, L. N., & Ghahari, S. A. (2021). Application of Digital Image Correlation in Structural Health Monitoring of Bridge Infrastructures: A Review. *Infrastructures*, *6*(12), Article 12. https://doi.org/10.3390/infrastructures6120176

Raissi, M., Perdikaris, P., & Karniadakis, G. E. (2019). Physics-informed neural networks: A deep learning framework for solving forward and inverse problems involving nonlinear partial differential equations. *Journal of Computational Physics*, *378*, 686–707. https://doi.org/10.1016/j.jcp.2018.10.045

Rathod, V. T., & Ramuhalli, P. (2022). Physics-informed neural networks for identification of material properties using standing waves. *Nondestructive Characterization and Monitoring of Advanced Materials, Aerospace, Civil Infrastructure, and Transportation XVI*, *12047*, 179–188. https://doi.org/10.1117/12.2607314

Sotiras, A., Davatzikos, C., & Paragios, N. (2013). Deformable Medical Image Registration: A Survey. *IEEE Transactions on Medical Imaging*, *32*(7), 1153–1190. https://doi.org/10.1109/TMI.2013.2265603

Thirion, J.-P. (1998). Image matching as a diffusion process: An analogy with Maxwell's demons. *Medical Image Analysis*, *2*(3), 243–260. https://doi.org/10.1016/S1361-8415(98)80022-4

Zitová, B., & Flusser, J. (2003). Image registration methods: A survey. *Image and Vision Computing*, *21*(11), 977–1000. https://doi.org/10.1016/S0262-8856(03)00137-9